An Experimental Investigation of Oil Recovery Mechanisms and Relative Permeability Curves Obtained by Steady-State versus Unsteady-State Displacement

Bashir Alkhazmi[1]*, *Amir* Farzaneh[1] *and Mehran* Sohrabi[1]

[1]Centre for Enhanced Oil Recovery and CO2 Solutions, Institute of GeoEnergy Engineering, Heriot-Watt University, Edinburgh, UK.
[1]*Currently with BP Exploration Operating CO., Sunbury, UK.

Abstract. Steady-state (SS) and unsteady-state (USS) coreflood experiments are performed in laboratories to obtain data and information that are critical to predicting multiphase flow in subsurface oil and gas reservoirs. These include relative permeability (kr) curves and trapped hydrocarbon saturation. Generally speaking, steady-state experiments take a relatively long time to do compared to their unsteady-state counterparts. For that reason, the unsteady-state experiments are performed as the industry standard. However, the unsteady-state experiments have several limitations including a relatively narrow saturation range for which kr curves can be obtained, particularly when in-situ saturation monitoring (ISSM) is not available. There has been much debate in the literature about the comparison of the results of these two different types of multiphase flow experiments and whether or not they should produce the same kr and trapped phase saturation, but the jury is still out. Part of the difficulty in comparing the results of the experiments is that there are a number of hard to define and control parameters that affect the results of these coreflood experiments including wettability of the rock and its possible changes during the experiments. In this paper, we present the results of two well-controlled coreflood experiments that were performed to generate reliable data and compare the results of steady-state experiments with unsteady-state experiments in a long sandstone core. The core was aged in a crude oil prior to running the experiments, and to minimise the change of wettability during the experiments, a live oil phase made from an equilibrium mixture of C1 and C4 was used. Two-phase water/oil flow (SS) and displacement experiments (USS) were performed under the pressure of 1840 psi and a temperature of 100°F. To assist with analysis of the results of the experiments, the coreflood rig was equipped with an x-ray in-situ saturation monitoring system. Comparing steady-state and unsteady-state results for the conditions of our coreflood experiments revealed that the remaining oil saturation (Sor) was 10% higher in the steady-state experiment than that in the unsteady-state experiment. Although the oil relative permeability (kro) curves obtained from steady-state and unsteady-state experiments were almost identical for Sw ≤ 30%, the unsteady-state kro values became higher and the gap between unsteady-state kro and steady-state kro increased when approaching the remaining value of oil saturation. The dominate mechanism by which the incremental oil was recovered during each fractional flow in steady-state experiment was by banking up the oil with different magnitudes corresponding to the increase in the water fractional flow ratios and the remaining oil saturation inside the rock. The results shed more lights on the mechanisms of multi-phase flow in porous material and provides a valuable suite of experimentally obtained data.

1 Introduction

The phenomenon of two-phase water-oil flow occurs within oil reservoirs when the two phases (oil and water) become mobile. Several flow modes have been identified in the literature for two-phase water-oil system including co-current, countercurrent, steady-state, unsteady-state and transient (e.g. imbibition & drainage). This type of immiscible flow has been broadly encountered in many applications of hydrocarbon recovery process, including primary oil recovery (or depletion) where both phases can simultaneously flow under steady-state conditions (deep in oil reservoirs and/or if pressure at the drainage boundaries of a well is maintained constant while the well is producing), secondary oil recovery (e,g. water flood, flow of aquifers into the oil zone by pressure maintenance, etc.) and tertiary oil recovery (e.g first WAG slug). During secondary and tertiary recovery processes, oil is displaced by water front under unsteady-state conditions.

The pore-scale mechanisms and the actual flow of an immiscible two-phase fluid in a porous media were first discussed by Richards [1]. He proposed a long-standing assumption that in the immiscible steady-state flow regime the oil flows only through interconnected

* Bashir Alkhazmi: bashir.alkhazmi@yahoo.co.uk

pathways, whereas the disconnected oil remains stationary. Honarpour and Mahmood [2] agreed with this assumption and suggested that when a phase becomes discontinuous at its finite saturation, its effective permeability becomes zero. However, many other authors did not fully support this assumption and directed their efforts to studying the contribution of the disconnected oil to the substantial flow of oil within the pore spaces. Hence, since then, the motion of the disconnected oil ganglia (droplets/clusters) has been experimentally [3]–[8] and theoretically [9]–[11] (investigated. In addition, some numerical work was directed to the steady state flow regime such as the pore-scale Lattice-Boltzmann [12] and the network simulations at larger scales [13].

Since this paper is based mostly on experimental work, the focus will be directed further on the experimental studies that visually observed the motion of the disconnected oil ganglia. Payatakes [14] reported that, in the case of two-phase oil-water steady-state displacement, the trapped oil blobs/ganglions can still be mobilized if the increase in the wetting-phase (water) viscous force is enough to raise its interstitial velocities to a level that is high enough to mobilize the surrounded oil ganglia. Avraam and Payatakes [6]–[8] reported experimental results on a 2-D porous medium. Based on their visual observation, they classified the two-phase flow regime under steady-state conditions as follows: (i) in the case when oil flows in the connected pathways, the oil phase maintains its hydraulic connectivity along the length of the porous rock, whereas its relative permeability (k_{ro}) remains relatively high and does not change much with the flow rate of the wetting phase; (ii) in the case when oil flows through ganglion dynamics, the oil phase is disconnected into large ganglia, small ganglia and tiny ganglia (trapped inside the pores), whereas k_{ro} remains relatively low and is distinctly affected by the water flow rates. Both these flow regimes are strongly dependent on several parameters, including the capillary number, flow rate ratio, viscosity ratio and wettability [15] [7], [16].

During ganglion dynamic flow, the population of disconnected oil ganglia is subject to breakup and coalescence [6], [16]–[20]. However, it was found that the numbers of stranded oil ganglia increase in a system when capillary number and local pressure gradient decrease. Since the viscous forces are responsible for the mobilization of this ganglion population, these forces are proportional to the maximum length of the ganglion and the local pressure gradient. Hence, the gradual increase in the wetting fractional flow by increasing its viscous force will assist some of the multi-sized ganglion to meet each other and coalescence in the same pore. If water splits these connected ganglia into two thin filaments, water will drag oil from these threads into its flowing stream until these oil threads eventually collapse. The dynamic breakup takes place more frequently at low water saturation. In addition, the interactions between ganglia (collisions followed by coalescence, remobilizations of stranded ganglia, etc.) occur less frequently at relatively high water saturation. In contrast, Datta [21]observed that, for two-phase flow of steady-state imbibition, the oil phase slightly reconfigures its respective flow path each time the fractional flow of the wetting-phase (Q_w/Q_{total}) increases. This means that oil flows in new pathways, which contradicts the findings of many other studies that suggest oil only flows in unchanging connected paths when its fractional flow (Q_o/Q_{total}) is decreased.

Eleri [22] reported the results of a series of two-phase and three-phase coreflood experiments performed under steady-state (SS) and unsteady-state (USS) conditions and on Berea and Clashach sandstone cores. Their results showed that there was an 8 % difference in the end-point average fluid saturation between steady-state and unsteady-state displacement experiments. Thus, the oil-water relative permeability values were different between SS and USS. Unlike the displacement in the dynamic (unsteady state) situation, the steady-state front is not affected by instability. Reynolds [23] reported an experimental investigation of pore-scale behaviour of a core-scale SS flow conducted under reservoir conditions. They came up with a previously unobserved type of SS flow behaviour, termed ‘dynamic connectivity’, in which the flow of the non-wetting phase takes place through a network of connections that are continuously rearranged between filled pores. They also observed that the dynamic connectivity does not necessarily need the connections of the pathways to be established throughout the length of the core, as it also occurs through the interactions between the ganglion populations.

By conducting the two-phase (oil-water) steady-state forced imbibition (2φSSFI) and the two-phase (oil-water) unsteady-state forced imbibition (2φUSSFI) experiments as well as running numerical simulation using 3RP Sim, we aimed to generate reliable experimental data that cover a broader range of oil-water saturation points and their corresponding relative permeability values, firstly, to characterise the flow, mechanisms and physics underlying oil recovery by the forced imbibition process, at core scale, under steady-state and unsteady-state conditions. Secondly, to investigate any potential differences between steady state and unsteady state displacements in terms of fluid/flow characteristics properties as stated above. Thereby, if differences in fluid/flow parameters are identified, which is the case in this study, how these differences will affect the measurement, trends and end-points of the relative permeability curves and subsequently what possible impact of these different relative permeabilities would have on numerical simulation results, especially the predictions of oil and water recoveries. Finally, based on the outcomes from the above investigations, it would be possible to verify the validity of the use of the widely applied methodology by petroleum/reservoir engineers, that suggests to use SS-k_r as a replacement of USS-k_r or vice versa, in simulation, to predict water and oil recovery profiles of an oil reservoir.

2 Coreflood Set-Up, Materials and Methodology

2.1 Coreflood Set-Up

Fig. 1 illustrates a schematic diagram of the closed-loop coreflood rig that was employed to perform all core flood experiments presented in this paper. This coreflood comprises two main control units: X-ray monitoring system and coreflood facility and was designed to handle high-pressure and high-temperature (HPHT) conditions, in order to allow injection and production of gas, oil and water in steady-state and/or unsteady-state manner. During both experiments, all fluids were systematically injected in the wellbore to formation direction.

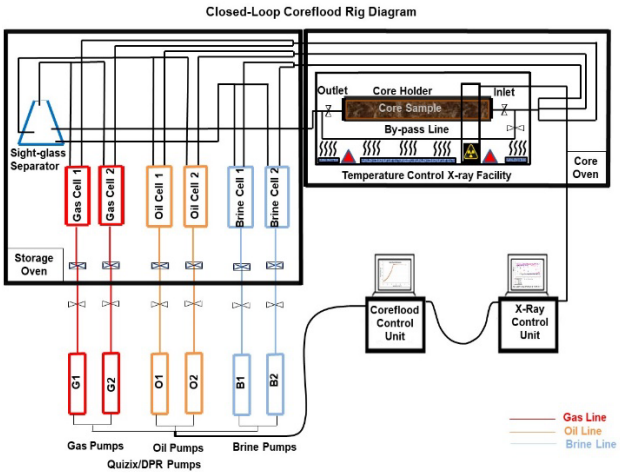

Fig. 1. Schematic diagram of the coreflood rig, including X-ray saturation monitoring system and coreflood control unit.

2.2 Materials

2.2.1 Rock

To eliminate the impact of the experimental artefacts (e.g. capillary end effects), a large (2 ft long x 2 in diameter) homogenous Clashach sandstone core was employed for this study. The base parameters of this core including porosity and permeability were measured at 18 % and 65 mD respectively, as shown in the schematic diagram in Fig. 2. During all the stages of the coreflood experiments presented in the paper, the core was horizontally-oriented and rotating at calculated number of revolutions per minute (rpm) to eliminate the effect of gravity.

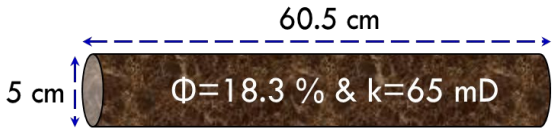

Fig. 2. Schematic diagram of Clashach sandstone core used in all of the coreflood experiments presented in this research paper.

Pore Structure. Because accurate description of the internal pore structure of a rock is crucial for the characterization of fluid flow/propagation in porous media and interpretation of the experimental results, especially for the conditions of steady-state and unsteady-state displacements, we carried out various types of investigation tests at different scales, including miscible tracer, Mercury Injection Capillary Pressure (MICP), X-ray scan analysis, Computed Tomography (CT) scan and Environmental Scanning Electron Microscope (ESEM) analysis on our Clashach sandstone core. The results of all these tests were consistent and assured a homogenous and clean sandstone rock with intergranular porosity. Further discussions on these investigation tests can be found in our former publication [24], [25].

Wettability. Both coreflood experiments (SS & USS) were conducted on the same wettability conditions of weakly water-wet. This was confirmed by Capillary Pressure and USBM Wettability Index Measurements, ESEM analysis and repeatability check (conducted pre- and post-SS experiment). It is worth mentioning that we previously presented the results of 2φUSSFI in a weakly water-wet system versus its USS counterparts obtained from the same 65 mD sandstone core with two different wettability conditions; water-wet and mixed-wet. Details and discussions on the effect rock wettability on the performance of water flood can be found elsewhere [26].

Capillary Pressure and USBM Wettability Index Measurements. A set of two-phase oil/water capillary pressure (P_c) data were generated for the 65 mD weakly water-wet Clashach sandstone core. The two Pc_{o-w} curves were directly measured using the porous-plate approach and represented by 1st drainage and 1st imbibition processes, as shown in Fig. 6 [28]. The USBM approach measures the work required for fluid (water/oil) displacement. Donaldson [29] used the logarithm of the ratio of the areas, obtained from primary drainage and imbibition capillary pressure curves, to measure the wettability index (WI). They tabulated the wettability regime based on a range of WI values, and hence, the rock wettability is identified as the following: water-wet when $0 < WI < 1$, intermediate wettability when $WI = 0$ and oil-wet when $0 > WI > -1$. Based on this classification, the wettability system of the 65 mD Clashach sandstone core was weakly water-wet, corresponding to measured wettability index value of 0.18 which was calculated from the areas under their primary drainage and imbibition capillary pressure curves, as presented in Fig. 6.

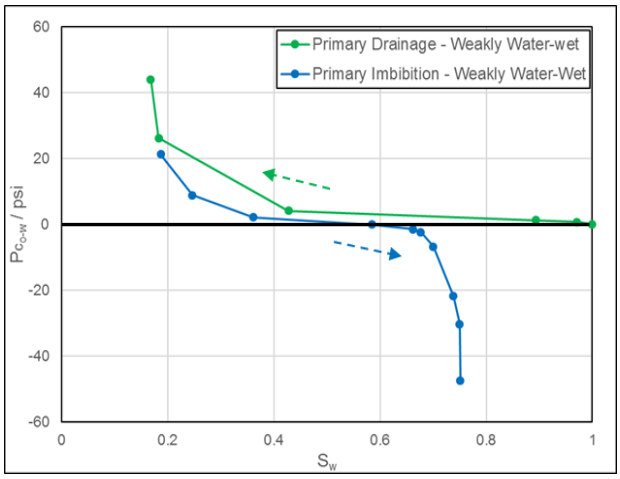

Fig. 3. A set of two-phase oil/water 1st imbibition and 1st drainage capillary pressure curves for 65-mD Clashach sandstone core under weakly water-wet conditions.

This approach strongly agreed with the wettability status of weakly water wetness determined by the ESEM analysis, as will be discussed below. It is worth mentioning that the imbibition Pc values have also been

used as inputs to 3RP Sim (three phase relative permeability simulator) to history match the ISSM, pressure drop and production data obtained from the two-phase unsteady-state coreflood experiment to generate reliable water-oil relative permeability data.

Environmental Scanning Electron Microscope (ESEM). For an accurate assessment of the rock wettability, a direct visualization into the micropores of the treated rock chip using an ESEM imaging technique was utilized. Sample was visually inspected for wettability using an XL30 ESEM and following the procedures of previous authors. In the ESEM procedure, thin slices of the sandstone were prepared and placed on a Peltier cooling stage, where they were cooled to 5˚C for 30 minutes to ensure equilibrium of the sample. The pressure was slowly raised to 0.125 psi (6.5 Torr), allowing condensation of water vapour on to the sample surface to assess wettability.

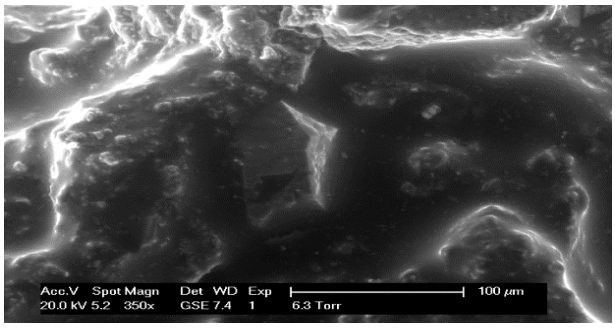

Fig. 4. ESEM image of sandstone chip, illustrating smaller pores filled with water in the weakly water-wet sandstone rock.

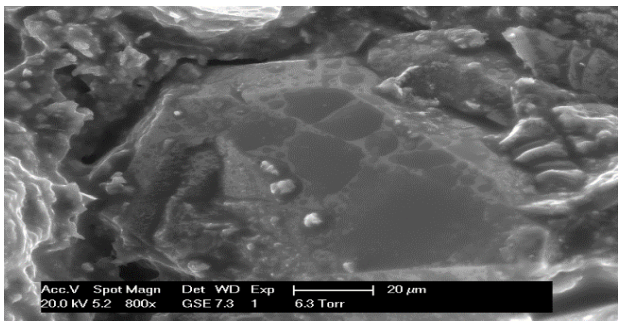

Fig. 5. ESEM image of small pores on rock chip, illustrating grain surface (quartz overgrowth) with a strong water wetness in the weakly water-wet sandstone rock.

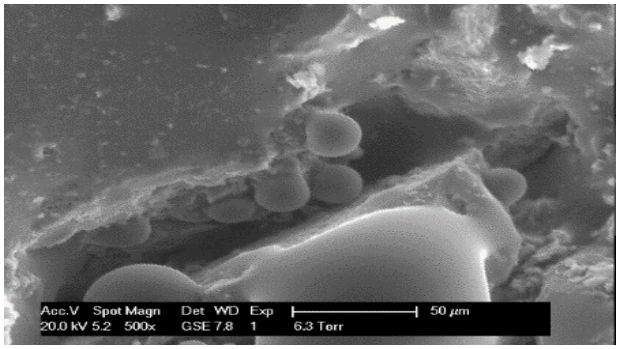

Fig. 6. ESEM image of rock grain in a rock chip, illustrating weakly water-wet conditions (middle bottom on quartz) and

Water was observed to imbibe through pores, forming thin films on grain surfaces (Fig. 3), indicating that the sandstone is water wet. Water condensed directly on to quartz overgrowth surfaces, forming irregular patches with extremely low contact angles (Fig. 4), indicating a strongly water wet character. Many other areas, which are covered in clays, exhibit much higher contact angles (Fig. 5), indicating more hydrophobic surfaces.

2.2.2 Fluids

Brine. The water phase with total salinity of 10,000 ppm was prepared by dissolving Sodium Chloride (NaCl) and Calcium Chloride (CaCl2) at a ratio of 4 to1 into distilled and vacuumed water and used as a flood water together with the immobile water phase in all coreflooding. The physical properties of this brine at 38 ºC are as listed in Table 1. Since brine may react with clay minerals coating some of the grain surfaces and result in clay swelling, which, in turn, would cause a blockage of some of the smaller pores inside the core, the composition of the brine was carefully designed to prevent any possibility of this reaction taking place and consequently eliminate any restriction of fluid flow within the porous medium.

Hydrocarbon. The hydrocarbon fluid system was prepared from a binary mixture of 73.6 mole percentage methane and 26.4 mole percentage n-butane at 2,250 psi and 38 ºC. The pressure of the hydrocarbon mixture was reduced to the test pressure of 1840 psia at the same temperature of 38 ºC. Then, the gas and the oil phases were separated in their respective storage cells. Only oil and water were mixed together at the test conditions (1840 psia and 38 ºC) to pre-equilibrate them prior to each displacement test. At these conditions, the corresponding oil-water interfacial tension (IFT) was measured at 41 $mN.m^{-1}$, which generates an immiscible front between oil and water phases during the displacement experiments. The measured density and viscosity values of this oil are as shown in Table 1.

Table 1. Physical properties of the fluids measured at 38 ºC and used in this study.

Phase	ρ ($kg.m^{-3}$)	μ (mPa.s)
Oil	317.40	0.0405
Water	992.96	0.680

2.3 Methodology

2.3.1 Coreflood Experiments

Two coreflood experiments are reported in this paper. Water was flooded through the 65-mD weakly water-wet sandstone core in a two different flow manner; steady-state and unsteady-state. Both coreflood experiments were conducted at the same reservoir conditions; 1840 psia and 38ºC and corresponding to oil-water IFT of 41 $mN.m^{-1}$ (± 2 $mN.m^{-1}$).

Prior to commencing each forced imbibition experiment, the core sample was cleaned, dried and vacuumed. Then, the immobile water saturation, S_{wim}, was established at 18 % using a series of mineral oils and normal alkanes (Fig.

7). The 2φSSFI experiment started by co-injecting water and oil into the core at water and oil ratios of 1 % and 99 % respectively (Table 2: IR-1). Even, after detecting the breakthrough, the injection ratio was maintained until the pressure drop across the core became stable and no change occurred in the fluid saturations, mainly because the injection and production rates were equal.

Table 2. Fractional flow and injected pore volume corresponded to different injection ratios during 2φSSFI experiment.

Injection Ratios	Fractional Flow, %		Injected Pore Volume (PVi)	
	Oil	Water	Oil	Water
IR-1	99	1	41.86	0.42
IR-2	98	2	21.86	0.44
IR-3	97	3	12.24	0.37
IR-4	96	4	12.36	0.51
IR-5	60	40	3.65	2.43
IR-6	40	60	3.17	4.76
IR-7	32	68	3.08	6.56
IR-8	20	80	2.21	8.86
IR-9	12	88	0.76	5.6
IR-10	4	96	0.40	9.55
IR-11	0	100	0	12.90

After these equilibrium conditions were attained and uniform propagations of fluids were established across the core, the injected water/total fluid ratio was raised to 2 % and the same procedure was repeated (Table 2: IR-2). The water fractional flow was gradually increased using the same strategy until this experiment was completed (Table 2: IR-1 – IR-10).

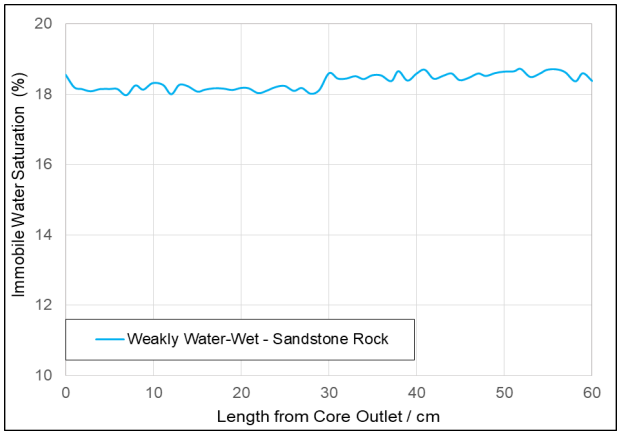

Fig. 7. Average immobile water saturation profile along the length of the weakly water-wet Clashach sandstone rock measured for each coreflood experiment presented in this paper.

Since only water was injected in the last injection ratio (Table 2: IR-11), oil was directly displaced by water front under displacement conditions of unsteady state. The latter injection ratio was carried out to obtain the end points (S_w, S_o, k_{rw} & k_{ro}). In the 2φUSSFI experiment, water was flooded through the core sample at the total rate till water broke through and oil production reached to practically zero. Detailed discussions regarding two-phase flow and displacement mechanisms under unsteady-state conditions in sandstone rock can be found elsewhere [26], [30], [31]. It is worth mentioning that both 2φSSFI and 2φUSSFI were conducted at the same total flowrate which is equivalent to the waterfront advancement velocity of 5 ft/day on the field scale. The latter injection flowrate was carefully selected after was being found to create a stable flow and eliminate gravity segregation and experimental artefacts. At the end of each core flood experiment a multi-rate water pumping was performed to investigate the impact of artefacts (e.g capillary end effects, dead volume, etc) on our experimental results and it has been observed that insignificant additional oil (hold up at the end face) corresponded to the pump flood periods. This reveals that there is no significant effect of the experimental artefact on the oil recovery and fluid saturations of our experiments. To simplify the comparisons of the methodologies for both coreflood experiments, schematic diagrams are used, as an example, to illustrate the different fractional flow stages (during 2φSSFI) and the different time steps of water injection (during 2φUSSFI), as shown in Fig. 8.

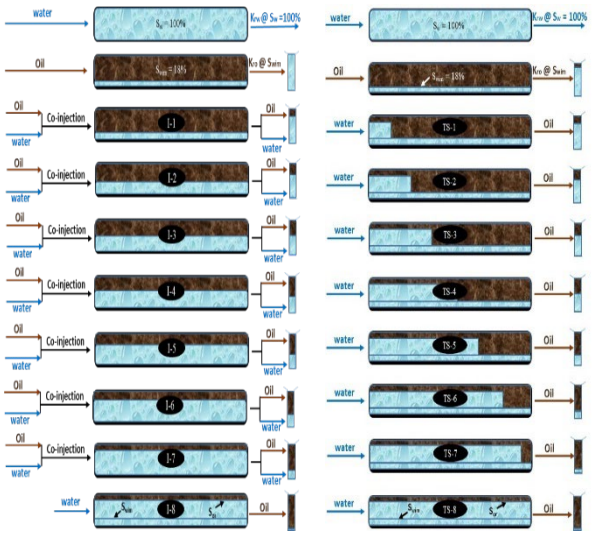

Fig. 8. Schematic diagrams compare the experimental methodologies between 2φSSFI (left graph) and 2φUSSFI (right graph). The 2φSSFI graph simulating the preparation stage (brine & oil injections) and different fractional flow stages (from I-1 to I-8) whereas the 2φUSSFI graph emulates the preparation stage (brine & oil injections) and water flood versus time steps (from TS-1 to TS-8).

2.3.2History Matching Using 3RPSim

The Heriot-Watt in-house software, 3RPSim, together with the data obtained from unsteady state coreflood experiment which was performed in EOR research group are used to estimate two-phase relative permeability and capillary pressure. Eclipse reservoir simulator is used as the coreflood simulator linked to 3RPSim. The in-house software 3RPSim (3-phase Relative Permeability Simulator) was developed as an optimization tool to obtain two- and three-phase relative permeability from unsteady-state displacement test results by trying to match the ISSM and measured pressure-production data, using a Genetic Algorithm (GA). The program gives best

estimates of two- and three-phase flow functions (kr and Pc) based on suitable mathematical functions defined to describe their dependency on phase saturations.

Fig. 9 shows the schematic workflow chart of the estimation approach for two-phase system, which consists of three segments: kr and Pc functions, core flood simulator, and GA optimization Algorithm. Either Eclipse-100 or 300 (black oil or compositional) simulators can be used within the 3RPSim to simulate the 1-D coreflood experimental data. Therefore, all features and mechanisms available in Eclipse can be applied for simulation of the coreflood experiment to obtain two-phase kr and Pc in an iterative process. The optimization starts with an initial guess for the kr and Pc (if unknown) functions as input to the core simulator. The difference between experimental and modelling results, referred to as misfit (objective error function), is minimized iteratively by automatically adjusting the parameters of kr and Pc functions until a small error tolerance is achieved.

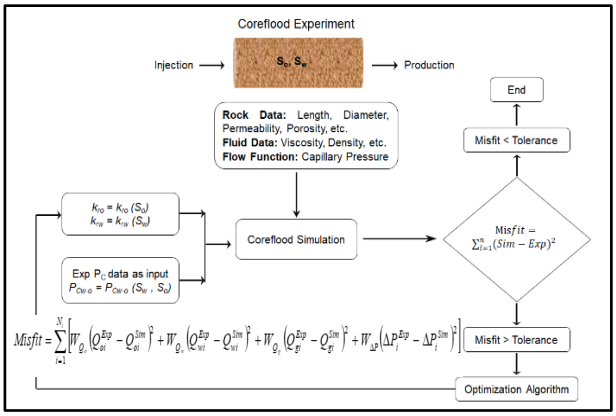

Fig. 9. Workflow for determination of two-phase kr from unsteady state coreflood experiment.

In the current study, because the two-phase oil-water capillary pressure function (Pc) was directly measured in the laboratory, as presented in Fig. 6, the threshold pressure value and a range of Pc values obtained from the imbibition curve were provided to 3RPSim as inputs. Having experimental measurements for a set of imbibition and drainage Pc data including threshold pressure and maximum capillary pressure have improved the uniqueness of the history matching results. In addition, this assessed in minimizing the number of iterations as well as the running time by only adjusting the kr parameter automatically. In this simulator the genetic algorithm has been used as an optimization procedure to minimize the objective function attempting to find the global minimum absolute value of the misfit. Further discussion on the history matching procedure including the inclusion of ISSM date can be found elsewhere [32]–[34].

3 Results and Discussions of Steady-State Two-Phase Relative Permeability Experiment

3.1 Effect of Steady-State Displacement on Fluid/Flow Characteristic Properties

3.1.1 Two-Phase Flow and Trapping Mechanisms

Fig. 10 shows a schematic representation of the actual flow and trapping mechanisms of oil by water during the steady-state two-phase (water-oil) forced imbibition experiment concluded from this study and several other coreflood studies and 2-D & 3-D glass-etched micromodels (using quasistatic and fast synchrotron X-ray CT techniques) reported in the literature ,as discussed earlier, in the introduction. The diagram illustrates the following: the co-injection of water and oil (q_w & q_o), tortuous flow of the connected oil pathways (COP), the connected water pathways (CWP), the oil ganglia breakup (OGB), the oil ganglia coalescence (OGC) and the dynamic flow of the multisized oil ganglion (MOG) population. In addition, due to the co-injection of oil and water, oil maintains its hydraulic continuity throughout the core in the presence of the displacing fluid (water). According to the above-mentioned publications[6], [16], [20], the size of the continuous oil path may get shrunk corresponding to the increase in the water saturation inside the core and the water/oil injection ratio.

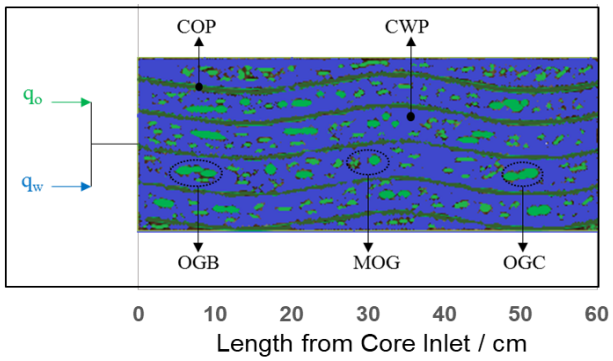

Fig. 10. Schematic representation of the actual flow and trapping mechanisms under steady-state and two-phase (water-oil) conditions of a forced imbibition test. RGB colour coding is used: green represents oil and blue represents water.

3.1.2 Oil Recovery and Differential Pressure

Fig. 11 shows the oil recovery performance and pressure drop behaviour corresponding to 154 PV of water-oil co-injection (upper graph) and 52.5 PV of injected water (lower graph) under steady-state imbibition conditions in a weakly water-wet sandstone core. As can be seen from the figure the upper graph illustrates an extension of the area of the early injection stages between IR-1 and IR-4 whereas the lower graph shows an extension of the area of the subsequent injection ratios, from IR-5 to IR-11.

Investigating the oil recovery profile from both graphs reveals that the highest oil recovery, of 29.65 % (IOIP %), was achieved by the first injection ratio (IR-1). Oil recoveries of 20.35 % (IOIP %) from the subsequent injection ratios (IR-2 to IR-10) were essentially from oil banks of different magnitudes formed ahead of the waterfronts, corresponding to the increase in the injection ratios when switching from one ratio to another as well as the remaining oil inside the core after each injection ratio. Hence, the ultimate oil recovery achieved by the two-phase steady-state forced imbibition (2φSSFI) experiment was 50 % (IOIP %).

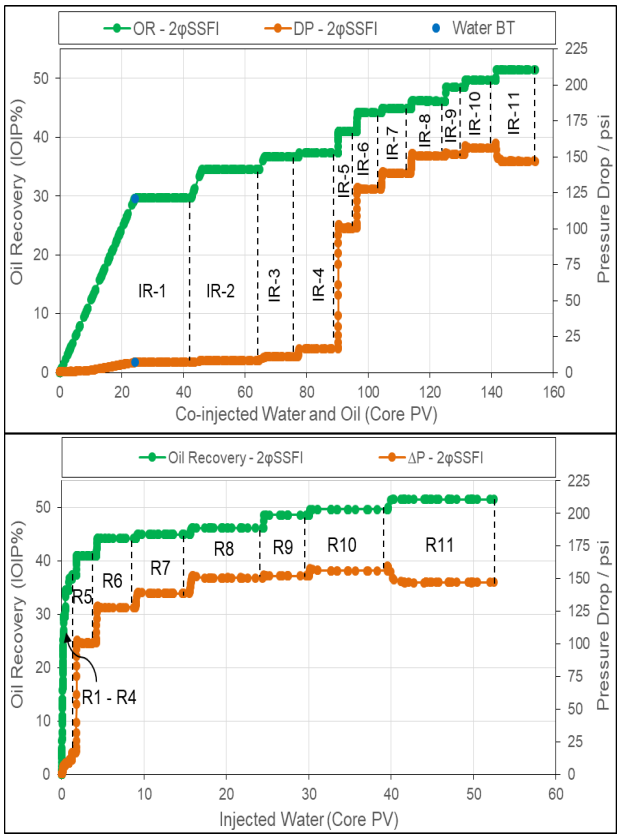

Fig. 11. Cumulative oil recovery and pressure drop plotted against co-injected water and oil (upper graph) and injected water (lower graph) corresponding to different injection ratios of the simultaneous injection of water and oil during the two-phase steady-state forced imbibition (2φSSFI) relative permeability experiment.

Pressure drop (DP) values increased gradually, corresponding to the increase in the injection ratios and water saturation inside the core. During the first four injection ratios (IR-1 to IR-4), DP trends were increasing at relatively lower rates. However, the DP values during the 5th fractional flow (at IR-5) increased dramatically (at higher rate), corresponding to the increase in the water fractional flow by a factor of 10 (from 4 % to 40 %) and its saturation level (Sw = 48.58 %) inside the core when the injection ratio switched from IR-4 to IR-5.

3.1.3 Average Fluid Saturation Profiles

The effect of the forced imbibition process on the average water and oil saturations inside the core under steady-state displacement conditions was investigated for the weakly water-wet sandstone core, as shown in Fig. 12. The initial average saturations of water and oil inside the core were S_{wim} = 18 % and S_{oi} = 82 %. With the start of IR-1, oil saturation decreased at an almost constant rate, corresponding to the increase in water saturation inside the core until water broke through at the core outlet. In the subsequent injection ratios (IR-2 to IR-10), the total water saturation gradually increased corresponding to the productions of small oil banks formed ahead of the waterfronts. The narrow saturation range of 18 % (42% ≥ S_w ≤ 60%) obtained from the 2φSS relative permeability experiment can be attributed to the effect of water-oil viscosity ratio.

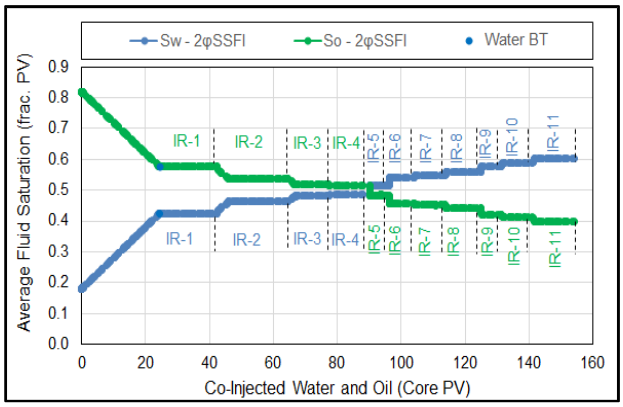

Fig. 12. Average water-oil saturations corresponded to different injection ratios of water-oil co-injection during two-phase steady-state forced imbibition (2φSSFI) relative permeability experiment.

Comparing the Fig. 12 with Fig. 11 revealed that the highest reductions in the average So associated with higher injectivity (lower ΔP) values corresponded to the injection ratios from IR-1 to IR-4, where the water-oil saturation level was at the intersect saturation point (S_w = S_o = 50 %). At the end of 2φSSFI experiment, the final S_w inside the core increased to 60 % whereas the oil saturation correspondingly dropped to 40 %.

3.2 Steady-State Water-Oil Relative Permeability Curves

The modified Darcy's law, as described below, was used to calculate the water-oil relative permeability values for each fractional flow when the fluid flow conditions reached equilibrium/steady-state:

$$\frac{Q_w}{A} = -\frac{k\, k_{rw}}{\mu_w}\frac{\partial P_w}{\partial x} \quad (1)$$

$$\frac{Q_o}{A} = -\frac{k\, k_{ro}}{\mu_o}\frac{\partial P_o}{\partial x} \quad (2)$$

where, Q is the volumetric flow rate, k is the absolute permeability of the medium, k_r is the relative permeability of the medium to a flowing phase, μ is the fluid viscosity and ∂P is the pressure drop of each phase across the test core sample. The indices of 'w' and 'o' stand for the water and oil phases, respectively. Using the above equations, the effective permeabilities of water and oil are calculated. The relative permeability of the flowing water and oil phases at given saturation levels are calculated as follows:

$$k_r = \frac{k_{eff}}{k_{abs}} \quad (3)$$

Fig. 13 (upper graph: full linear scale and lower graph: semi-log scale) illustrates the water-oil relative permeability bounding curves generated from a two-phase steady-state forced imbibition experiment conducted on a weekly water-wet sandstone rock sample. As can be observed from both graphs, measured steady-state k_{ro} and k_{rw} values are both quite low and changing within a narrow water saturation range (of about 18 % S_w). This may be attributed to the effect of oil/water viscosity ratio (μ_o/μ_w = 0.0595).

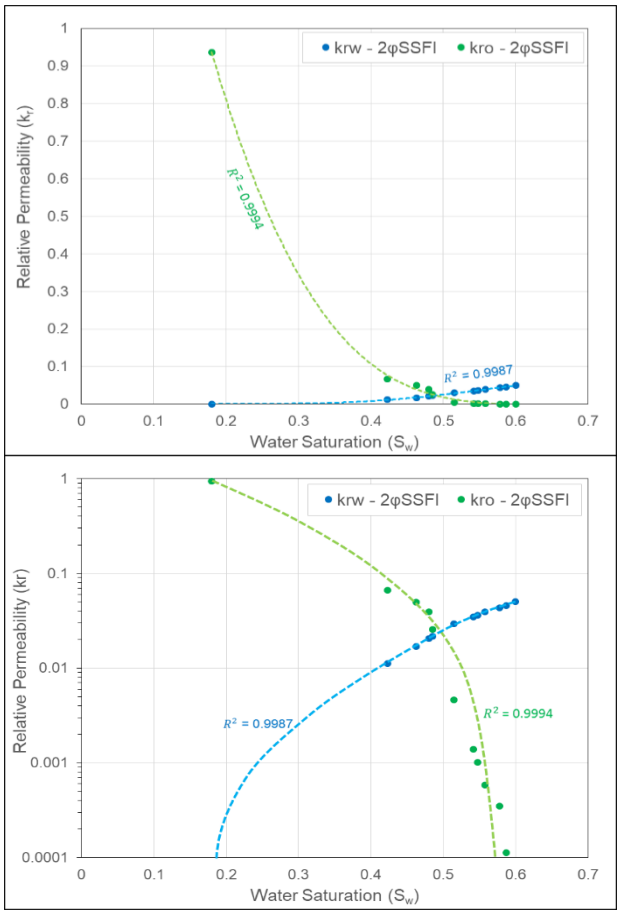

Fig. 13. Measured two-phase oil-water steady-state forced imbibition relative permeability data (Upper graph: full linear scale; Lower graph: semi-log scale).

3.3 Repeatability Check for Possible Wettability Alteration after Steady State Flow Period

To check the possible alteration in the core wettability, a water flood post-SS was conducted and used as a key experiment to check the wettability status after the 2φSSFI experiment was complete, as shown in Fig. 14.

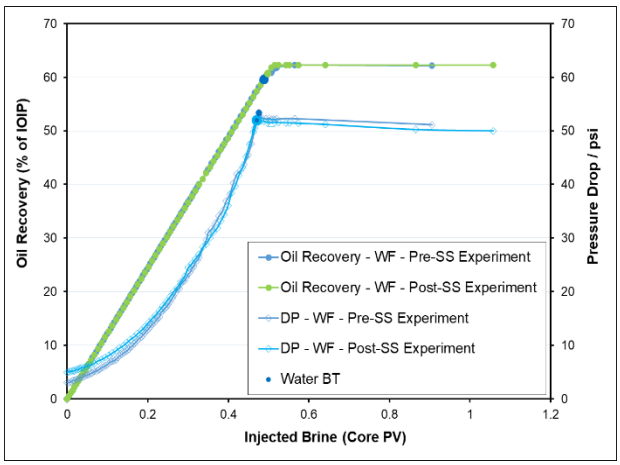

Fig. 14. Comparisons of oil recoveries and pressure drops corresponded to water flooding under weakly water-wet conditions before and after steady state experiment.

The post-SS water flood was a repeat to the 2φUSSFI and it was performed before the SS experiment. By comparing the performance of water floods (pre-SS versus post-SS) in terms of oil recoveries and pressure drops it can be concluded that the trends from both experiments were almost identical, which demonstrates no change on the core wettability and an excellent repeatability of wettability check.

4 Comparisons of Coreflood Results: Steady State versus Unsteady State

4.1 Comparisons between X-ray In-situ Saturation Monitoring Profiles in Steady State and Unsteady State.

Fig. 15 depicts the in-situ saturation monitoring profiles obtained from 2φUSSFI and 2φSSFI experiments using X-ray scanning analysis. In this study we report a full in-situ saturation monitoring (ISSM) profile for USS experiments, whereas for SS experiment, only the first four fractional flow periods are reported. The ISSM profiles were obtained using a number of equally distributed slices in the axial direction, as though the core was scanned slice by slice at a series of time points.

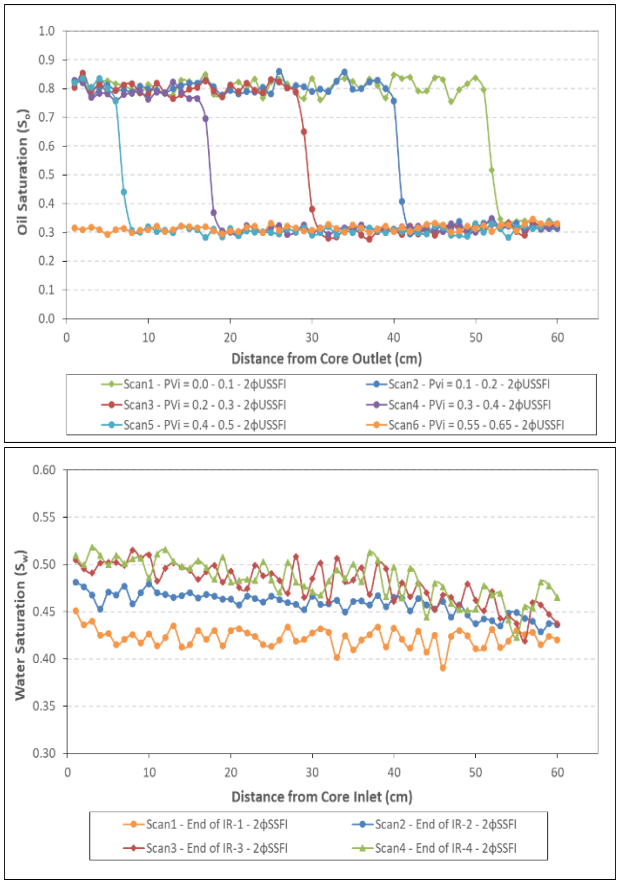

Fig. 15. In-situ saturation monitoring profiles obtained from 2φUSSFI (upper graph) and 2φSSFI (lower graph) experiments using X-ray scanning analysis.

As can be seen from the above graphs, for the USS profile (upper graph), a stable piston like displacement front was generated by the advancing waterfront along the length of the core sample indicating that there are no major heterogeneities (no fracture or shale, etc) in the core. In addition, the graph shows the change in the local oil

saturations at different injected pore volume (PVi) intervals, or time steps, across the rock sample. The local remaining oil saturation at the end of scanning was measured at 33 % which is in a very good match the one obtained from the average saturation profile (at 41.2 %) using material balance calculations. For SS profile (lower graph), apart from some normal fluctuations, the in-situ S_w values are relatively the same along the core, with smaller reduction as approaching the core outlet. The local in-situ S_w values from SS were also matching those values presented above in the global saturation profile. Both in-situ saturation profiles of SS and USS experiments confirm the reliability and accuracy of the experimental data used in the comparisons between SS and USS in this study.

4.2 Effect of Displacement Experiments on Oil Recovery

To investigate the efficiency of oil recovery under two-phase steady-state (2φSS) and two-phase unsteady-state (2φUSS) displacements in a weakly water-wet sandstone rock, the oil recovery trends obtained from both forced imbibition experiments (2φSS & 2φUSS) were plotted together against the PV of the injected water, as shown in Fig. 16. In this plot, overall oil recovery is included and calculated as a percentage of initial oil in place (IOIP %), whereas Fig. 17 shows the oil recovery as a percentage of the remaining oil to water after the first injection ratio (IR-1) during the 2φSSFI relative permeability experiment. Because there was no oil recovery (slope is at zero) after 0.9 PV, extrapolated data points (up to 51.5 PV) were added to the water flood recovery trend (of 2φUSS), in order to facilitate its comparison with that obtained from 2φSS forced imbibition.

As can be seen from Fig. 16, oil recovery performance by USS water flooding is considerably higher than that by its SS imbibition flood counterpart. Ultimate oil recoveries of 62 % (IOIP %) were achieved by the USS water flood, whereas the SS imbibition flood achieved only 51.5 %. In addition, the time taken for water to prematurely break through in the SS imbibition flood (at 0.243 PV) was almost half that required in the USS water flood (at 0.475 PV). Furthermore, only 6.82 % (S_{orw} %) of oil was recovered immediately after water breakthrough under unsteady-state displacements, whereas about 28.3 % (S_{orw} %) of additional oil was produced by multi-point steady-state imbibition displacements (Fig. 17). Based on all the above findings, the better oil recovery performance in the USS than in SS displacement may be explained by the nature of the differences in the type of displacement occurring in SS and USS. Thus, it can be concluded that the oil recovery mechanisms by water injection under either type of displacement (SS or USS) is significantly affected by a number of parameters, such as injection strategy, fluid injection ratio, remaining oil saturations and capillary number. Under weakly water-wet conditions, the injected water would represent the wetting phase characteristics associated with quartz, in which the oil displacement at microscopic scale is dominated by 'a corner filament flow', whereas if a rock surface had a clay lining, water would be a non-wetting phase or weakly-wetting phase and, hence, oil displacement would be approaching a piston-like type.

Under unsteady-state displacement, when water was flooded into the core, it formed its facial front at the core inlet, which then moved ahead towards the core outlet at a relatively stable sweeping efficiency. This led to oil being produced at high and constant rates, due the direct displacement of oil by water. The small curvature of oil recovery observed after water BT (at 0.475 PV) and prior to production ceasing (at 0.52 PV) may be attributed to a slow oil drainage through a conductive flow path of oil layers. This characteristic was previously reported for mixed-wet and weakly water-wet systems [35]–[37]. Relying on Darcy's theory, only a few reliable relative permeability values can be obtained at their saturation levels from this very narrow curvature.

The actual flow profile under steady-state conditions is much more complex compared to that of unsteady state. When water, at low ratio, is flooded simultaneously with oil during the steady-state imbibition process, water and oil separately establish their respective flowing streams between the core inlet and outlet (refer to Fig. 10). Due to the systematic increase in water ratio after equilibrium was attained at each fractional flow, the local pressure and viscous force of water would correspondingly increase. This would mean that oil may be recovered by different displacement mechanisms, depending on; the water/oil injection ratio, remaining oil saturation and the acting viscous forces of water and oil. Hence, the small recovered oil banks (from IR-2 to IR-10) throughout the steady-state experiment may be attributed to three main recovery mechanisms. Firstly, water was establishing new displacement paths along the length of the core as further injection ratios were carried out. Secondly, the formerly established water flow paths became thicker after the oil ratio and saturation were decreased. Thirdly, some of the trapped oil in the larger pores was dragged out towards the core outlet due to the increase in the interstitial pressure and viscous force of the water phase compared to that of oil. The latter recovery process of oil is referred to as steady-state ganglion dynamics (as discussed in the introduction).

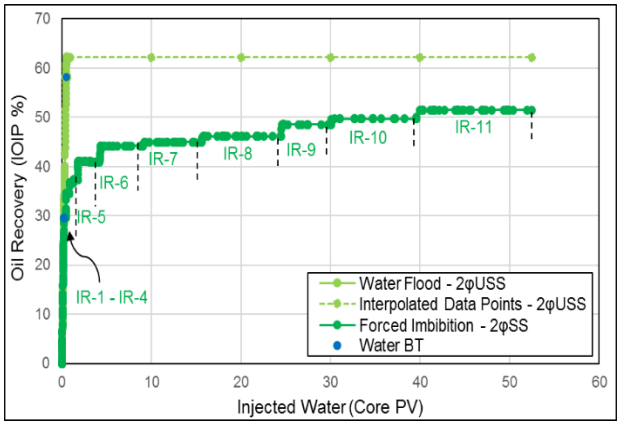

Fig. 16. Comparison of oil recovery efficiency obtained from forced imbibition processes of two-phase steady-state and unsteady-state displacements.

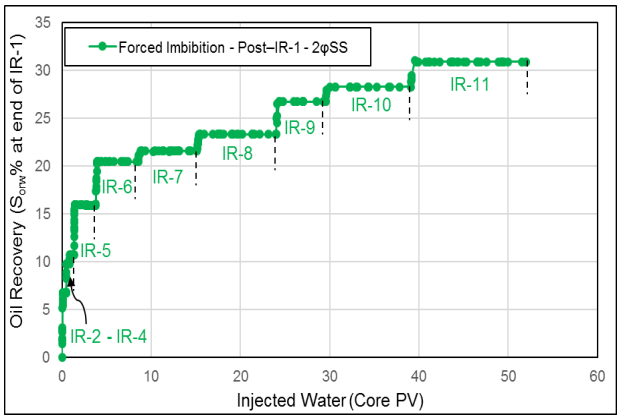

Fig. 17. Oil recovery performance after 1st injection ratio (IR-1) during the two-phase steady-state forced imbibition (2φSSFI) relative permeability experiment.

4.3 Effect of Displacement Experiments on Pressure Drop

Fig. 18 illustrates the behaviour of corresponding pressure drop (ΔP) for 2φSSFI and 2φUSSFI displacements. As can be observed from the graph, the ΔP values at the end of the multi-point SS forced imbibition (at IR-10) are larger, by a factor of about three, than those obtained by the USS water flood. As a result, the loss in the injectivity values, which are in an inverse proportion to ΔP values, of water in the SS imbibition flood will be three times greater than that obtained from USS water injection.

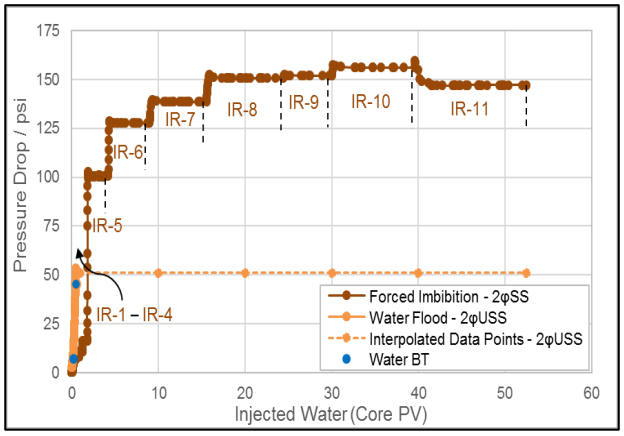

Fig. 18. A comparison of pressure drop behaviour obtained from forced imbibition processes of two-phase steady state and unsteady state displacements.

The latter observed behaviour may have a manifold explanation: firstly, the large increase in ΔP values in 2φSSFI corresponded to the increase in the water fractional flow, by a factor of 10, when the injection ratio of water increased from 4 % (at IR-4) to 40 % (at IR-5). Secondly, the adverse effect of each phase on the injectivity of the other phase during the simultaneous injections of water and oil is a well-identified problem in this type of SS imbibition flood, due to the high pore-scale competition between water and oil in which each phase tends to invade more new pores. Thirdly, the increase in the trapped oil saturation (S_{or}) by 10 % in SS compared to its USS counterpart may have a role in the increase in the SS-ΔP values. Finally, taking into account the fact that the water viscosity (0.68 cp) is higher than oil viscosity (0.0405 cp) by a factor of about 17 and the increase of the average water saturation (S_w) to 50 % (confirmed by the local value from X-ray in-situ saturation monitoring profile) inside the core sample at the start of IR-5, will act to increase the average all weighted fluid viscosity inside the rock that may be contributed in the increase of the SS-ΔP values.

4.4 Effect of Displacement Experiments on Water-Oil Relative Permeability Curves

To examine the degree of uncertainties associated with the unsteady-state water-oil relative permeability values, obtained by history matching techniques, a steady-state imbibition coreflood experiment was performed to generate more reliable water-oil relative permeability curves, as shown in Fig. 19. Comparing oil relative permeabilities shows that, at higher water saturation ($S_w \geq 40$ %), all the k_{ro} values obtained from the unsteady-state experiment are much higher than their values measured under steady-state conditions. In addition, all the k_{rw} values obtained from the unsteady-state experiment are much lower than their values measured under steady-state conditions.

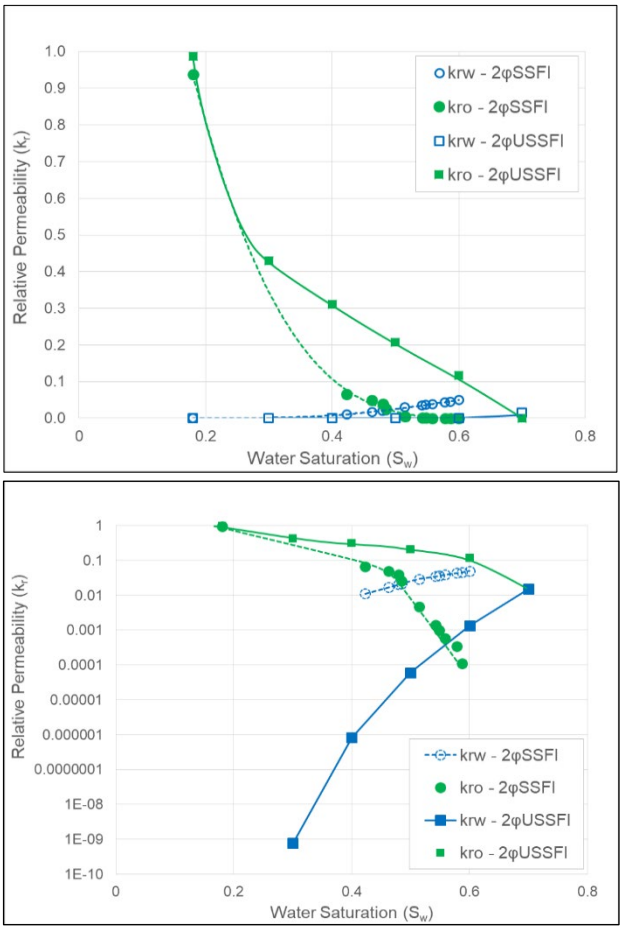

Fig. 19. A comparison of water (blue) and oil (green) relative permeability curves obtained from steady-state (dashed lines) and unsteady-state (solid lines) coreflood experiments. Top graph: linear scale and bottom graph: semi-log scale.

It should be mentioned that while the SS kr curves shown in Fig 19 were measured directly, the USS kr curves were

obtained indirectly and by history matching the differential pressure and the fluid production data obtained during the unsteady state displacement experiments. There will be some uncertainties and error involved in the process of extracting kr by the history matching process. Unfortunately, we are unable to quantify or to present the goodness of the history matched data here due to unavailability of this data.

During the unsteady-state imbibition displacement experiment, in this weakly water-wet system, water was initially advancing through the smaller pores and then through the larger ones, with better conductivity, as well as through the voids, by the least resistant paths (to establish its respective phase saturation path along the core) towards the core outlet. This type of flow had caused some large oil-filled pores to be by-passed by water, and the trapping of oil to be increased within the core throughout this experiment. Thus, comparing this type of experiment to that of steady state, as presented in Fig. 19, shows that the fluid flow conditions and the trapping mechanisms of the non-wetting phase are different between steady-state and unsteady-state displacements.

The greater the entrapment of the non-wetting phase (oil), the greater is the reduction of its relative permeability. In other word, as can be observed from Fig. 19, when the SS-k_{ro} is compared to its unsteady-state counterpart, considering that $S_{o,rem}$ is 10 % higher in SS than that of USS, the k_{ro} curve in USS had shifted up compared to that obtained by SS and, as a result, the use of SS-k_{ro} as a substitution to USS-k_{ro} would under estimate the predicted oil recovery by reservoir simulator. In addition, the two-phase SS ΔP values across the core seem to be governed by water viscosity (0.68 mPa.s) than oil viscosity (0.0405 mPa.s), which would result in a greater reduction in the k_{ro} values. Thus, oil relative permeability, k_{ro}, values obtained by the steady-state flooding were low for limited oil saturation levels inside the core.

5 Conclusions

The following conclusions can be drawn from the coreflood experiments that were performed on 65 mD weakly water-wet Clashach sandstone core under steady-state and unsteady state displacements.

- Ultimate oil recovery of 50 % (IOIP %) was achieved by the two-phase steady-state imbibition coreflood experiment. About 29.65 % (IOIP %) of this was due to a large oil bank formed ahead of waterfront at the infinitesimal rate (IR-1). The essential mechanism by which the 20.35 % (IOIP %) of incremental oil was recovered during the subsequent fractional flow (IR-2 – IR-10) was by oil banks with different magnitudes, corresponding to the increase in the water/total injection ratios and the remaining oil saturation inside the rock.
- Comparing the trapped oil saturations shows that the remaining oil saturation ($S_{o,rem}$) obtained from steady-state displacement is almost 10 % larger than its value measured in the unsteady-state experiment. This difference in $S_{o,rem}$ was measured in some other core flood studies in the literature which suggested that the impact of this difference on water-oil relative permeability curves is negligible. On the contrary, for the conditions of our experiment, our results revealed that this difference in the end points is significant and has shifted up the k_{ro} curve, and shifted down the k_{rw} trend of USS measurements compared to their SS counterpart.
- Comparing the two oil relative permeability curves reveal that the values obtained from the unsteady-state coreflood experiments, using history matching technique, are much higher than the values obtained by the steady-state technique. The replacement of unsteady-state k_{ro} curve with that obtained from steady state in simulation would result in an underestimation of the predicted oil recovery.
- Comparing water relative permeability data illustrate that the water relative permeability values measured by unsteady-state experiment are much lower than the ones obtained by the steady-state experiment. As a result, replacing them in simulation with those obtained from steady state would overestimate the predicted water recoveries.
- The data seem to suggest an inherent difference in the nature of fluid displacement during SS and USS coreflood experiments. As a result, it can be said that the recovery mechanisms and their corresponding water and oil relative pemeabilities under two-phase flow conditions are significantly different between SS and USS displacement experiments.

References

1. L. A. Richards, Physics, *Capillary Conduction of Liquids Through Porous Mediums*, **1 (5)**, 318–333, doi: 10.1063/1.1745010. (1931).
2. M. Honarpour and S. M. Mahmood, J. Pet. Technol., *Relative-Permeability Measurements: An Overview*, **40 (08)**, 963–966, doi: 10.2118/18565-PA. (1988).
3. K. M. Ng, H. T. Davis, and L. E. Scriven, Chem. Eng. Sci., *Visualization of blob mechanics in flow through porous media*, **33 (8)**, 1009–1017, doi:10.1016/0009-2509(78)85004. (1978).
4. S. RapinAPIN, MSc thesis, University of Houston, *Behavior of non-wetting oil ganglia displaced by an aqueous phase*. (1980).
5. A. C. Payatakes and M. M. Dias, *Rev. Chem. Eng.*, *Immiscible Microdisplacement and Ganglion Dynamics in Porous Media*, **2 (2)**, doi: 10.1515/REVCE.1984.2.2.85. (1984).
6. D. G. Avraam and A. C. Payatakes, *Transp. Porous Media, Generalized relative permeability coefficients during steady-state two-phase flow in porous media, and correlation with the flow mechanisms*, **20 (1–2)**, 135–168, doi: 10.1007/BF00616928. (1995).
7. D. G. and A. C. P. Avraam, J. Fluid Mech., *Flow*

Regimes and Relative Permeabilities during Steady-State Two-Phase Flow in Porous Media, **207–236**, 293. (1995).

8. D. G. Avraam and A. C. Payatakes, Ind. Eng. Chem. Res., *Flow Mechanisms, Relative Permeabilities, and Coupling Effects in Steady-State Two-Phase Flow through Porous Media: The Case of Strong Wettability*, **38 (3)**, 778–786, doi: 10.1021/ie980404o. (1999).
9. A. C. Payatakes, K. M. Ng, and R. W. Flumerfelt, AIChE J., *Oil ganglion dynamics during immiscible displacement: Model formulation*, **26 (3)**, 430–443, doi: 10.1002/aic.690260315. (1980).
10. M. M. Dias and A. C. Payatakes, J. Fluid Mech., *Network models for two-phase flow in porous media Part 2. Motion of oil ganglia*, **164**, 337–358, doi: 10.1017/S0022112086002586. (1986).
11. G. N. Constantinides and A. C. Payatakes, J. Colloid Interface Sci., *A theoretical model of collision and coalescence of ganglia in porous media*, **141 (2)**, 486–504, doi: 10.1016/0021-9797(91)90346-A. (1991).
12. A. K. Gunstensen and D. H. Rothman, J. Geophys. Res. Solid Earth, *Lattice-Boltzmann studies of immiscible two-phase flow through porous media*, **98 (B4)**, 6431–6441, doi: 10.1029/92JB02660. (1993).
13. T. Ramstad and A. Hansen, *Phys. Rev. E*, *Cluster evolution in steady-state two-phase flow in porous media*, **73 (2)**, doi: 10.1103/PhysRevE.73.026306. (2006).
14. A. C. Payatakes, Annu. Rev. Fluid Mech, *Dynamics of Oil Ganglia During Immiscible Displacement in Water-Wet Porous Media*, **14 (1)**, 365–393. (1982).
15. B. Gutiérrez, F. Juarez, L. Ornelas, S. Zeppieri, and A. L. de Ramos, Int. J. Thermophys*, Experimental Study of Gas–Liquid Two-Phase Flow in Glass Micromodels*, **29 (6)**, 2126–2135, doi: 10.1007/s10765-007-0305-9. (2008).
16. K. Tallakstad, Phys. Rev. Lett, *Steady-State Two-Phase Flow in Porous Media: Statistics and Transport Properties.*, **7**. (2009).
17. G. N. Constantinides and A. C. Payatakes, AIChE J., *Network simulation of steady-state two-phase flow in consolidated porous media*, **42 (2)**, 369–382, doi: 10.1002/aic.690420207. (1996).
18. A. . Valavanides, M.S., Constantinides, G.N. & Payatakes, *Transp. Porous Media, Mechanistic Model of Steady-State Two-Phase Flow in Porous Media Based on Ganglion Dynamics*, **30***,* 267–299, doi: 1006558121674. (1998).
19. K. Tallakstad, G. Løvoll, H. Knudsen, T. Ramstad, E. Flekkøy, and K. Måløy, Phys. Rev. E, *Steady-state, simultaneous two-phase flow in porous media: An experimental study*. (2009).
20. A. G. Yiotis, L. Talon, and D. Salin, Phys. Rev. E, *Blob population dynamics during immiscible two-phase flows in reconstructed porous media*. (2013).
21. S. S. Datta, T. S. Ramakrishnan, and D. A. Weitz, Phys. Fluids, *Mobilization of a trapped non-wetting fluid from a three-dimensional porous medium*, **26 (2)**, doi: 10.1063/1.4866641. (2014).
22. O. Eleri, A. Graue, and A. Skauge, "*Steady-State and Unsteady-State Two-Phase Relative Permeability Hysteresis and Measurements of Three-Phase Relative Permeabilities Using Imaging Techniques*. (1995).
23. C. A. Reynolds, H. Menke, M. Andrew, M. J. Blunt, and S. Krevor, Proc. Natl. Acad. Sci., *Dynamic fluid connectivity during steady-state multiphase flow in a sandstone*, **114 (31)**, 8187–8192, doi: 10.1073/pnas.1702834114. (2017).
24. B. Alkhazmi, A. Farzaneh, M. Sohrabi, and A. Sisson, SPE Western Regional Meeting, SPE 190053, A*n Experimental Investigation of WAG Injection Performance under Near-Miscible Conditions in Carbonate Rock and Comparison with Sandstone*, doi: 10.2118/190053-MS. (2018).
25. B. Alkhazmi, M. Sohrabi, and A. Farzaneh, the 3rd SPE Kuwait Oil & Gas Show and Conference, SPE 187537, *An Experimental Investigation of the Effect of Gas and Water Slug Size and Injection Order on the Performance of Immiscible WAG Injection in a Mixed-Wet System*, doi: 10.2118/187537-MS. (2017).
26. B. Alkhazmi, A. Farzaneh, and M. Sohrabi, J. Buckman, SPE Annual Technical Conference and Exhibition, SPE 191477, *A Comprehensive and Comparative Experimental Study of the Effect of Wettability on the Performance of Near Miscible WAG Injection in Sandstone Rock*, doi: 10.2118/191477-MS. (2018).
27. T. Ahmed, Reservoir engineering handbook. (2010).
28. C. Lenormand, R., Eisenzimmer, A. & Zarcone, Symp. Soc. Core Anal., Int. no. SCA 9322 presented during the International Symposium of the Society of Core Analysts, Houston, TX, USA, *A Novel Method for the Determination of Water/Oil Capillary Pressures of Mixed Wettability Samples*. (1993).
29. E. C. Donaldson, R. D. Thomas, and P. B. Lorenz, Soc. Pet. Eng. J.,*Wettability Determination and Its Effect on Recovery Efficiency*, **9 (01)**, doi: 10.2118/2338-PA. (1969).
30. B. Alkhazmi, A. Farzaneh, and M. Sohrabi, SPE & 81st EAGE Annual Conference and Exhibition, SPE 195566, *A Thorough Coreflood Study of the Effect of Gas Viscosity and Cyclic Hysteresis on the Performance of Gas and WAG Injections under Near-Miscible Displacement Conditions in a Weakly Water-Wet Sandstone Rock*, doi: 10.2118/195566-MS. (2019).
31. B. A. A. Alkhazmi, *Investigation of Enhanced Oil Recovery by Water Alternating Gas (WAG) Injection in Sandstone and Carbonate Rocks*, Heriot-Watt University, Edinburgh, United Kingdom. (2019).
32. H. Shahverdi, *Characterization of three-phase flow and WAG injection in oil reservoirs*, Heriot-Watt University, Edinburgh, UK. (2012).
33. A. Jahanbakhsh, *Two- and three-phase flow functions for numerical simulation of EOR processes*, Heriot-Watt University, Edinburgh, UK. (2017).
34. A. Jahanbakhsh and M. Sohrabi, *A New Approach for Simultaneous Estimation of Relative Permeability and Capillary Pressure from Coreflood Experiments*, doi: 10.2118/175068-MS. (2015).
35. R. A. Salathiel, J. Pet. Technol., *Oil Recovery by Surface Film Drainage In Mixed-Wettability Rocks*, **25 (10)**. (1973).
36. M. Latil, *Enhanced Oil Recovery*. Technip Editions. (1980).
37. K. Singh, B. Bijeljic, and M. J. Blunt, Water Resour. Res., *Imaging of oil layers, curvature and contact angle in a mixed-wet and a water-wet carbonate rock*, **52 (3)**. (2016)**.**